Quaternary Geochronology 72 (2022) 101369

Contents lists available at ScienceDirect

Quaternary Geochronology

journal homepage: www.elsevier.com/locate/quageo

Late Quaternary evolution of lower reaches of the Volga River (Raygorod section) based on luminescence dating

N.A. Taratunina [a,*,1], J.-P. Buylaert [b], R.N. Kurbanov [c], T.A. Yanina [d], A.O. Makeev [d], M.P. Lebedeva [e], A.O. Utkina [f], A.S. Murray [g]

[a] Proizvodstvennaya St., 8/1, 119619, Moscow, Russia
[b] Department of Physics, Technical University of Denmark, DTU Risø Campus, DK-4000, Roskilde, Denmark
[c] Profsoyuznaya St., 104, 117437, Moscow, Russia
[d] Leninskie Gory St., 1, 119234, Moscow, Russia
[e] Pyzhevskiy per., 7/2, 119017, Moscow, Russia
[f] Vernadskogo St., 9, 119311, Moscow, Russia
[g] Department of Geoscience, Aarhus University, Høegh-Guldbergs Gade 2, DK-8000c, Aarhus, Denmark

ARTICLE INFO

Keywords:
Late Pleistocene
Lower Volga region
Caspian Sea
Luminescence dating
Paleogeography

ABSTRACT

The normally-closed Caspian Sea is known for large changes in relative sea-level (of ~170 m) during the late Quaternary. These transgressive/regressive events influenced the topography, sedimentation and ecosystems of a large area, of up to 1 million km^2. The Volga River has played an important role in the water balance of the Caspian Quaternary basins but our understanding of the temporal evolution is poorly constrained. Recent studies on the evolution of the Lower Volga have focused mainly on the subaerial sequence of loess-palaeosol series corresponding to a long-duration Caspian low stand (the so-called "Atelian regression" from ~90 to ~25 ka). In this study we address, for the first time, the temporal evolution of the Volga River during the late Quaternary, as recorded in the many layers of alluvial sands at the Raygorod reference section. This 50 m high outcrop contains a complicated sequence of different types of interlayered alluvium (channel and floodplain facies), a loess-palaeosol sequence with a weakly developed palaeosol, and marine sediments of the Khvalynian transgression (Chocolate Clay facies). The new chronology, based on 35 samples, is derived using optically stimulated luminescence (OSL) analysis of sand-sized quartz, with support from post-infra-red infra-red stimulated luminescence (post-IR IRSL) from K-rich feldspar grains to date the older parts of the section. The new ages identify five stages of the topography development in the northern parts of the Lower Volga: (1) an MIS 5a flood-plain in deltaic/estuary environments (>90 ka) during a high-stand of the Caspian Sea (Hyrcanian transgression); (2) a transition from deltaic/estuary conditions to a river valley with normal alluvial sedimentation and sporadic stabilization reflected in palaeosol development (80–70 ka); (3) a palaeo-Volga channel migration at elevations of 4–8 m msl during 69–62 ka, evidence of a brief increase in Caspian Sea-level and blocking of the Volga flow; (4) a subaerial stage with high-speed accumulation of loess during MIS 4 to MIS 2, containing one weakly developed palaeosol (MIS 3c) and pedocomplex of three combined palaeosols of the beginning of MIS2 (30–24 ka); (5) a rapid Khvalynian transgression, starting at the Raygorod location at ~18.3 ka, with relatively weak marine erosion of the top 40–60 cm of loess cover, presumably because of the rapid migration of the coastline in the flat Northern Caspian Lowland.

1. Introduction

The evolution of the natural environment of the Caspian region has long been under scrutiny (Grichuk, 1954; Goretskiy, 1966; Arslanov et al., 1988; Shkatova, 2010; Yanina, 2012, 2020; Tudryn et al., 2013; Svitoch, 2014; Lavrushin et al., 2014; Bolikhovskaya et al., 2017; Yanina et al., 2018; Badyukova, 2021). The Caspian Sea is recognised as a continentally and regionally important paleogeographical archive: a

* Corresponding author.
E-mail address: taratuninana@gmail.com (N.A. Taratunina).
[1] Please see acknowledgements.

https://doi.org/10.1016/j.quageo.2022.101369
Received 1 December 2021; Received in revised form 10 June 2022; Accepted 21 June 2022
Available online 30 June 2022

long history of sea-level fluctuations records the climate evolution of large parts of Central Eurasia and the water-balance dynamics of major rivers such as Volga, Kura, Terek, Amu-Daria and others. The main stages of the Caspian Sea evolution - the major transgressions – provide the stratigraphical basis for the Quaternary of Central Asia, Eastern Caucasus and the southern part of East European plain. The Lower Volga River valley is ideally suited for investigating the Pleistocene history of the Caspian Sea, and a series of sections has been characterized here over a long period of research (Fedorov, 1957; Vasiliev, 1961; Moskvitin, 1962; Svitoch and Yanina, 1997; Költringer et al., 2021; Kurbanov et al., 2021). These sections contain a unique record of the Quaternary history of the Caspian Sea, in the form of alternating marine and subaerial deposits.

Recently, researchers have been especially active on the Iranian coast, where the Holocene record is particularly complete (Leroy et al., 2011; Lahijani et al., 2007). In the east, in Turkmenistan (Kurbanov et al., 2014) and other locations, the history of the earlier stages of the Caspian history is, unfortunately, not yet fully described. Only recently were luminescence ages for the Hyrcanian (MIS 5) layers of the Manych depression obtained, providing a chronological framework for the connection of the Caspian Sea with the World Ocean during MIS 5 (Kurbanov et al., 2018). In the latest large international research into the stratigraphy of the Caspian Sea (Krijgsman et al., 2019) the Late Pleistocene is only very briefly discussed.

A number of questions concerning Caspian history remain unresolved, primarily due to the poor preservation of geomorphological evidence for the position of sea level. In this regard, the position of the Volga River channel and estuary (which are directly influenced by fluctuations in Caspian Sea level and the position of the coastline) play an important role in reconstructing the evolution of the Caspian Sea during the Late Pleistocene.

Reconstruction of the evolution of the Volga valley requires one to address several connected questions: (i) what are the most significant fluvial processes and how do these influence the development of the relief in the north of the Caspian Lowland? (i) How did the Volga River control sedimentation conditions in the North Caspian, in the Caspian Lowland, and in the deep bay which formed during the transgressive stages of the Caspian Sea. Despite the considerable attention given to the evolution of the natural environment of the Volga valley in its middle and lower reaches (Milanovskiy, 1932, 1940; Nikolayev, 1956, 1957; Goretskiy, 1966; Lower Volga, 2002, etc.), many unresolved issues remain. A particularly acute problem is the lack of a reliable chronology for the individual stages of the development of the valley.

In recent years, systematic studies have contributed to the first work on the structure of the loess-soil series in the Lower Volga region (Yanina et al., 2017; Lebedeva et al., 2018; Rogov et al., 2020; Taratunina et al., 2021; Makeev et al., 2021), and on their palaeogeographic significance (Bolikhovskaya et al., 2017; Yanina et al., 2021). Some initial climate reconstructions have also been carried out in the region (Bolikhovskaya et al., 2017; Költringer et al., 2020, 2021). However, these studies lacked reliable and detailed independent ages since they are based on only a few age-tie points so that a detailed reconstruction of loess-palaeosol formation through time was not possible.

Furthermore, due to the significant role of sea level in the formation of the relief of the Volga valley, Late Pleistocene alluvial terraces are not expressed in the Lower Volga. In contrast, in the Middle Volga, several terraces are distinguished (Makshaev, 2019; Makshaev and Svitoch, 2016), and all of them were affected by Caspian Sea level. Thus, it is impossible to understand the history of the lower Volga by analysing the geomorphological structure of the modern relief, because this relief was heavily modified by the Khvalynian (late MIS 2) transgression of the Caspian Sea; this transgression partially eroded any alluvial terraces, but more importantly covered them with a thick stratum of marine sediments, the so-called “Chocolate Clays” (Svitoch and Makshaev, 2015; Kurbanov et al., 2021). This makes any study of the alluvial deposits of the Late Pleistocene of particular importance.

In this paper we address the problem of the timing of the main alluvial/fluvial stages occurring during the development of the lower Volga valley, by examining the sediment record at the Raygorod section (Fig. 1). This contributes directly to our understanding of the relationship(s) of these stages with the transgressive-regressive events of the Caspian Sea, with glacial/interglacial events in the East European Plain, and with global climate change.

2. Study area

The study area is located in the southeast of the East European Plain, within the northwestern part of the Caspian Lowland (Fig. 1A,B). The Raygorod section is one of several sections reflecting the history of the development of the Caspian region in the Late Pleistocene is (Figs. 1 and 2, Habs 13.68 m, N 48.4313, E 44.9665). It is located on the right bank of the Volga River, 1 km east of the village of the same name. The section records the structure of the Early Khvalynian terrace of the Caspian Sea and, at the same time, it is a lectostratotype of the Atelian deposits of the Lower Volga region (Svitoch and Yanina, 1997; Arslanov et al., 2016). The sedimentary sequence (Fig. 1C) of the section is represented by deposits of alluvial, loessic and marine genesis, with a thickness of more than 21 m. The lower part of the section is represented by clayey deltaic deposits, gradually turning into interleaving loams and silts with layers containing traces of soil formation (Fig. 2, U21-14), and capped by a ~2 m thick unit of channel alluvium sands representing the top of the alluvial strata (U13). This lower part is overlain by a thick (7.5 m) loess-palaeosol sequence (Fig. 2, U12-5), containing 4 weakly developed palaeosols (Fig. 1C, No 11, 8–6). These subaerial sediments are in turn overlain, following a clear erosional boundary, by a unit of marine sediments represented by Chocolate Clays with numerous small interlayers of silts and sand (Fig. 1C, No 4–2; Fig. 2, U4-2). The structure of the section is completed by the Holocene soil formed in further subaerial sediments (Fig. 1C, No 1; Fig. 2, U1).

The Raygorod section differs significantly in its geomorphological position compared to other reference sections of the Lower Volga region (Srednyaya Akhtuba, Leninsk). The section is located between two Late Pleistocene Volga valleys - a well-defined modern and a more ancient valley laid along the Sarpinsky lakes (Nikolayev, 1957; Svitoch and Yanina, 1997; Lower Volga, 2002). The section is distinguished by its low elevation, which led to a prolonged and intensive accumulation of alluvial deposits, reflected in the lower ~8 m of alluvial sediments.

3. Luminescence sampling and measurement protocols

During fieldwork, sections were dug at Raygorod (Fig. 1C), and alluvial and loess-palaeosol sequences described and sampled for luminescence dating. The sediment is highly cemented and could not be sampled with tubes. Instead sampling was undertaken at night, when 45 intact blocks of consolidated material were cut and placed directly in non-transparent foil-lined plastic bags. Sample preparation took place under dimmed orange LED lights. Samples were processed using standard procedures: removal of potentially light-exposed surfaces, wet sieving to obtain very fine and medium sand fractions (63–90, 90–180 and 180–250 μm), treatment with 10% HCl, 10% H_2O_2, 10% HF, 10% HCl. This cleaning was followed by density separation of quartz/plagioclase and K-rich feldspar using a 2.58 g cm^{-3} LST FastFloattm aqueous heavy liquid solution with repeated washing using distilled water between each step. The heavier quartz/plagioclase fraction was further treated with 40% HF to obtain a clean quartz extract; this was followed by a final washing in 10% HCl. Unfortunately during the chemistry stage a group of samples from the middle part of the section (interval 670–850 cm) were exposed to a fire in the drying oven and so only 35 samples are discussed further.

Clean quartz and K-rich feldspar grains from all 35 samples were measured at the Nordic Laboratory for Luminescence Dating (Risø Campus, Denmark). All measurements were made on multi-grain

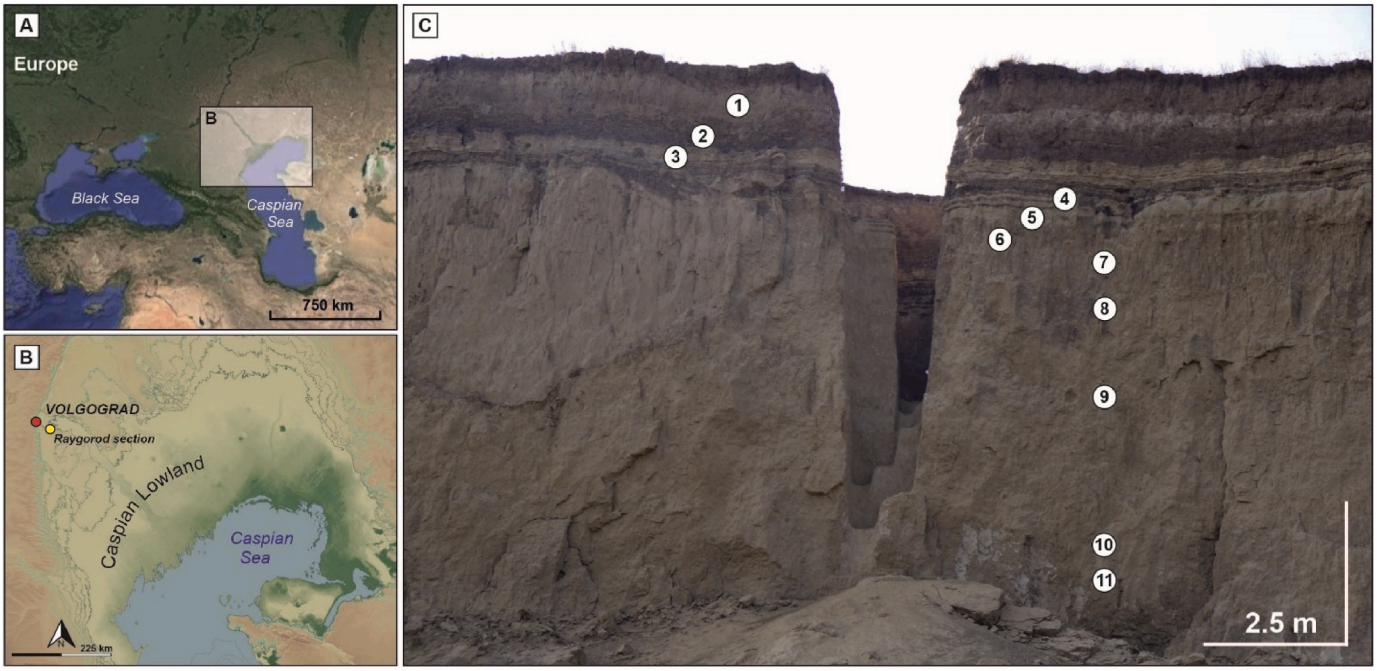

Fig. 1. The Raygorod reference section: A-B – location; C – photo of the top part of the section (the numbers indicate the layers in the schematic diagram in Fig. 2).

aliquots mounted on stainless steel discs (quartz, sample Ø ~8 mm) and stainless steel cups (K-rich feldspar, Ø ~2 mm), and measured in a Risø TL/OSL model DA-20 reader equipped with a calibrated beta source (Hansen et al., 2018). The quartz OSL signal was detected through a U-340 filter and K-rich feldspar post-IR IRSL through a blue filter combination (Thomsen et al., 2008).

Quartz purity checks were performed using an IR OSL depletion ratio test (Duller, 2003); the average OSL IR depletion ratio is 0.978 ± 0.004 (n = 195; 35 samples) compared to the standard blue recycling ratio on the same aliquots of 0.99 ± 0.003 confirming the luminescence purity of the quartz extracts. Quartz dose estimates were made using a standard SAR protocol with a 260 °C preheat for 10 s, a 220 °C cut heat and an elevated temperature (280 °C) blue-light stimulation at the end of each SAR cycle (Murray and Wintle, 2000, 2003). The quartz OSL signal was measured at 125 °C using blue light stimulation for 40; early background subtraction (first 0.32s minus subsequent 0.32s) was used for net signal calculations. K-feldspar dose estimates were measured using a post-IR IRSL SAR protocol (Buylaert et al., 2012) with preheat and cut-heat of 320 °C for 60 s and an IR stimulation at 200 °C (for 200s) followed by an IR stimulation at 290 °C (for 200s) ($pIRIR_{200,290}$; e.g., Li and Li, 2012; Yi et al., 2015). Late background subtraction was used for net $pIRIR_{200,290}$ signal calculation using the initial 2 s minus the last 50 s of the decay curve. No correction was made for $pIRIR_{200,290}$ signal instability (Buylaert et al., 2012, 2015; Yi et al., 2015; Stevens et al., 2018).

3.1. Dosimetry

Radionuclide concentrations were measured using high resolution gamma spectrometry and the calibration method is described in Murray et al. (1987, 2018). Samples were air dried, ground, ignited at 450 °C for 24 h, and mixed with high viscosity wax before casting in a cup-shaped mould. This process presents the sample to the detector in a fixed geometry and prevents the loss of radon gas. The resulting ^{226}Ra, ^{232}Th and 40 K activity concentrations were converted to dry infinite-matrix dose rates following Guérin et al. (2012). Water content corrections were as described by Aitken (1985) and cosmic ray contributions derived from Prescott and Hutton (1994). K-rich feldspar grains had an internal beta dose rate contribution added based on a measured K concentration of 12.7 ± 0.1% (n = 8, samples covering entire range of section) using a Risø XRF attachment (see e.g., Stevens et al., 2018). A small internal dose rate contribution from U, Th was also incorporated (0.10 ± 0.05 Gy/ka; Zhao and Li, 2005); the corresponding value for quartz was 0.02 ± 0.01 Gy/ka based on Vandenberghe et al. (2008).

The radionuclide activity concentrations are given in Table S1, together with the assumed lifetime averaged water content. Water content calculations are based on our understanding of the geomorphological evolution of the Volga valley, the influence of the Volga River and Caspian Sea level during the Late Quaternary, and laboratory measurements of alluvial sands and loess from the nearby section at Srednyaya Akhtuba (Højsager, 2019). Because the Volga River has down cut through the marine and loess deposits by 30–50 m, the long term average water contents are assumed to be significantly greater than those measured after excavation from the exposed river section. The section wall is being actively eroded by the river; during the last century the wall has retreated by at least 50 m. Clearly our section has been considerably more inland for most of its history. This affects its relationship with ground water; present day ground water in the Northern Caspian Lowland is found at a depth of ~8.5 m. For sediment below this level (units 12–18, Fig. 2) we have taken measured saturated water contents (ranging from 28 to 40%) to be most representative of the lifetime average. During most of the Late Quaternary the sea level was low and the river channel position was also relatively low, allowing the upper 8.5 m to be well-drained. Based on this information, we have assumed a lifetime average water content of 50% of saturation for this overlying loess/loam, giving a water content fraction by weight of 15 ± 5%. After the Khvalynian transgression the subaerial sediments were covered by the impermeable Chocolate Clay facies (unit 2, Fig. 2) causing a perched water table in the interleaved sands and the overlying Holocene material.

Total dose rates generally reflect the type of sediment: the smallest quartz dose rates are recorded in the alluvial sands (187779, −80), of 0.78 ± 0.01 to 1.07 ± 0.02 Gy ka^{-1} (random errors only); in loess values vary between 1.13 ± 0.02 (187,778) and 2.50 ± 0.04 Gy ka-1 (187,751); loess sediments also contain the largest dose rates in section. A clear trend in dose rate can be observed in loess between 970 cm and 860 cm: it gradually increases from the lower horizons with dose rates of 1.13 ± 0.02 (187,778) to ~2 Gy ka^{-1} (187,758) at the top. The top loess unit (200–600 cm) has a dose rate of ~2.40 Gy/ka.

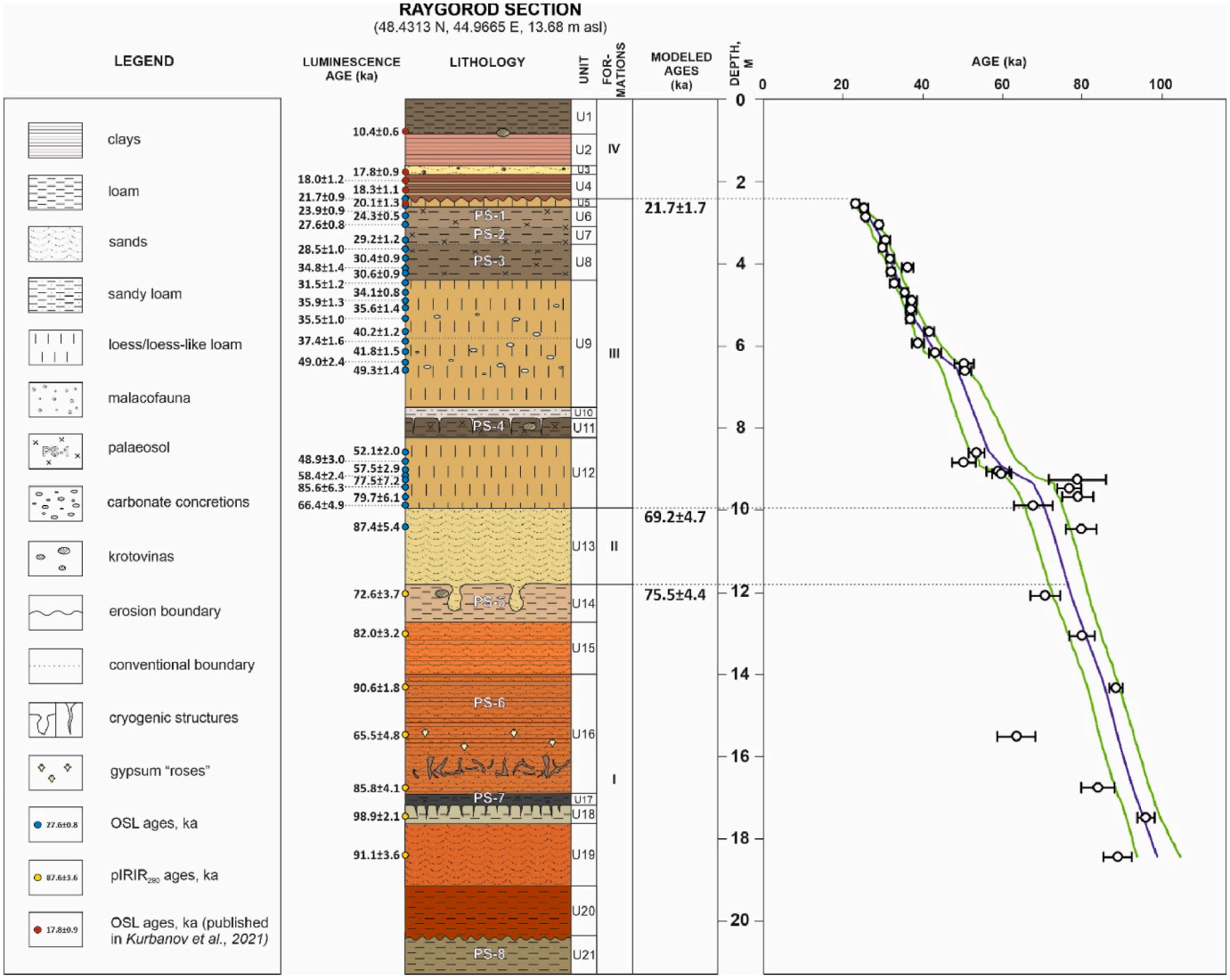

Fig. 2. Structure of the Raygorod reference section, luminescence ages and final Bayesian age model.

4. Results

4.1. Stratigraphy of the Raygorod section

The Raygorod section can be considered in terms of four main formations (Fig. 2) representing different formative processes.

The lowest formation consists of units 21–14 and is represented by a series of different facies, mainly floodplain alluvial sediments. At the base of the section, there is an alternating beige sandy loam and brown loam, dense, with an apparent thickness of more than 2 m (unit 21) and a dense light brown sandy loam (unit 20) with horizontal and cross-bedding structure and rare ferruginous spots, 1.2 m thick. Above, unit 19 is made up of medium-grained reddish-beige sand, 1.5 m thick. The upper border is clear, uneven, with traces of ferruginous growth. Unit 18 is a gray-beige loam, 0.4 m thick turning into dark gray (to black) loam, organic rich (unit 17), 0.2 m thick. The boundary between these units is complicated by dense vertical cracks (10–15 cm) of wedge-shaped structures. The overlying units 16 and 15 are reddish-brown loam with a nutty jointing, with ferruginous spots, and a large number of gypsum roses 2–4 cm in diameter. Unit 14 is a massive sandy beige loam, about 1.0 m thick, with white carbonate nodules and rare krotovinas.

This sequence (units 21–14) reflects the development of the valley during changing water levels in the Late Quaternary Caspian basin. The lower part of sediments (units 21–20) was apparently formed during ingression of the Caspian Bay into the Volga valley. The resulting estuary-like conditions allowed accumulation of alluvial material, mainly of floodplain facies, with a total thickness of about 8 m, reflecting a change from the stagnant regime of a relatively active river flood plain (unit 19) to the development of soil formation processes in floodplain sediments (e.g. unit 17) and the formation of differently pronounced soil horizons. We identify unit 21 as representing a deltaic environment, based on the considerable similarity with the modern analogue in the present-day Volga delta, with sediments of high organic content, enriched with macroscopic plant debris.

The next formation is represented by unit 13. Unit 13 is a fine and medium-grained beige sand, well sorted, poorly cemented, and taken to represent periglacial alluvium, the so-called "Akhtuba layers", as introduced into the Lower Volga stratigraphic scheme by Goretskiy (1958) and Moskvitin (1962).

Above the alluvium layers there is a thick loess-palaeosol sequence (units 12–5) which reflects continental development of the region. The material is a dense, porous, carbonate-rich fawn sandy loam, with columnar jointing. In certain layers (units 6, 7, 8, 11), soil formation horizons are darker, with small-block structure, with cutans along the edges, manganese smears, and rare krotovinas. The total thickness of the loess-soil series is 7.30 m. In the regional stratigraphic scheme (Svitoch

and Yanina, 1997), this loess unit is identified as the Atelian subaerial formation, characteristic of the Lower Volga sections (Költringer et al., 2020).

Above a clearly eroded boundary to the loess-palaeosol formation (III) there are the so-called Chocolate Clays with fine-grained sands. These sediments contain typical Early Khvalynian species of mollusks *Didacna protracta, D. ebersini, Dreissena rostriformis, Dr. polymorpha* (Kurbanov et al., 2021) with a total thickness of 1.75 m (units 4–2). This formation also contains the modern kastanozem soil developed on Holocene loams (0.85 m) (unit 1). A chronology for this formation has been presented elsewhere (Kurbanov et al., 2021).

In summary, formation III is taken to represent Atelian subaerial strata reflecting a period of continental development of the region during a deep regression of the Caspian Sea – the Atelian regression (Yanina et al., 2021; Krijgsman et al., 2019). These strata are represented by an alternation of loess and soil horizons. The uppermost formation IV begins with the Chocolate Clays reflecting the development of the Early Khvalynian transgression with normal Caspian salinity; this took place at the end of the Pleistocene (Kurbanov et al., 2021). The uppermost layer of the section records the most recent continental development of the region, post-Khvalynian, with the formation of the Holocene soil.

4.2. Quartz OSL ages

The quartz OSL signal of sand-sized grains from all samples is sensitive, and Fig. 3a inset shows the natural OSL signal compared with a decay curve from Risø calibration quartz (Hansen et al., 2018). This clearly shows that quartz from the Raygorod section is dominated by a fast component. Fig. 3a presents a typical dose response curve (sample 187,743) showing the accuracy of the sensitivity correction; the recycling and OSL IR depletion data points for this aliquot are indistinguishable from first regeneration dose point (open circle).

Quartz dose recovery was measured using 16 samples down the section. Samples were bleached twice for 100s with blue light at room temperature (with 10 ks pause in between) before giving a beta dose of 65 Gy. The dose recovery results indicate that our chosen SAR protocol is able to accurately measure doses given prior to heat treatment in these samples; the average measured to given dose ratio is 0.992 ± 0.010 (n = 48) (Fig. 3b).

A preheat plateau test shows that the D_e is insensitive to the thermal pretreatment and the sensitivity correction works well over a wide temperature interval (Fig. 3c and d) - the average recycling ratio over all aliquots is 1.001 ± 0.004 (n = 24) and the average recuperation for the same aliquots is 0.05 ± 0.02% of the natural. Based on the preheat plateau and dose recovery data, a preheat of 260 °C for 10 s and cut-heat of 220 °C was chosen to measure the equivalent doses.

The quartz D_e estimates (arithmetic averages; Guérin et al., 2015, 2017) obtained using our selected protocol are summarised in Table 1 together with the standard deviations on the means (standard errors) and the number of rejected and accepted aliquots used to calculate the mean. Aliquots were rejected if they did not intersect the dose response curve (natural in saturation) or using the interquartile range (IQR) criterion (Medialdea et al., 2014). The quartz ages are also presented in Table 1.

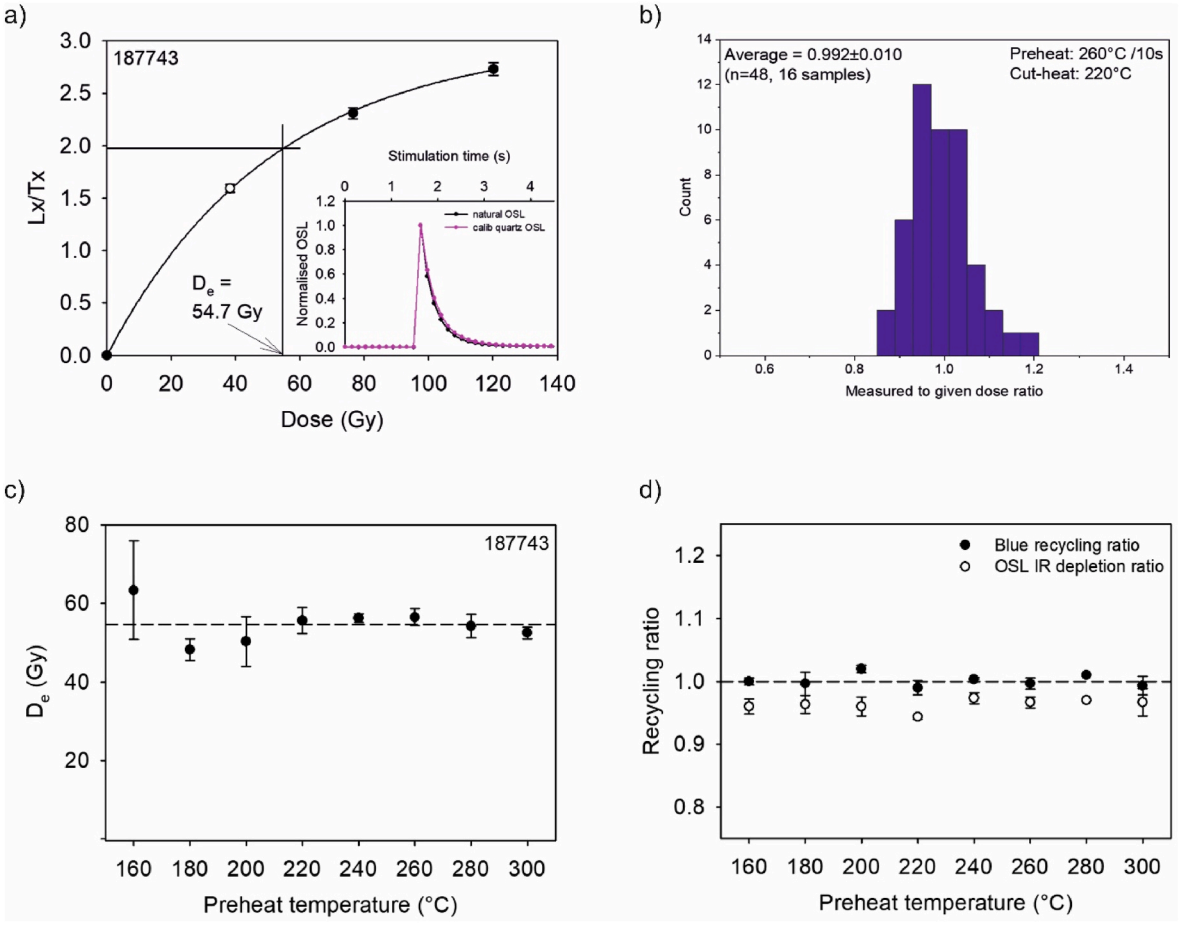

Fig. 3. Luminescence characteristics of quartz grains: a - typical quartz OSL dose response curve for sample 187,743; b - histogram of quartz dose recovery ratios for 16 samples down the section; c-d - quartz preheat plateau test.

Table 1
Quartz and K-feldspar luminescence results. Quartz and K-feldspar equivalent doses (D_e), total dose rates for K-feldspar grains, ages. Ages in bold were used for age-depth modelling. Resulting modeled ages using Bacon software. Age uncertainties represent one sigma and do not contain a systematic component.

Sample code	Depth (cm)	FK $pIRIR_{200,290}$			Quartz OSL			WC %	D_r^3	Age (ka)		Age ratio
		D_e (Gy)	n_r^1	n_a^2	D_e (Gy)	n_r	n_a		Gy/ka	FK $pIRIR_{200,290}$	Q OSL	$pIRIR_{290}/Q$
187,741	256	78 ± 3	0	9	52.5 ± 1.9	0	21	15	2.42 ± 0.04	25.5 ± 1.0	**21.7 ± 0.9**	1.2 ± 0.1
187,742	266	81 ± 3	0	6	58.7 ± 2.1	1	20	15	2.46 ± 0.04	26.1 ± 0.9	**23.9 ± 0.9**	1.1 ± 0.1
187,743	288	84 ± 2	0	6	60.4 ± 0.8	3	18	15	2.48 ± 0.04	27.0 ± 0.7	**24.3 ± 0.5**	1.1 ± 0.0
187,744	307	91 ± 1	0	9	68.6 ± 1.5	1	20	15	2.48 ± 0.04	31.5 ± 0.7	**27.6 ± 0.8**	1.1 ± 0.0
187,745	344	N.A.	0	0	73.1 ± 2.8	0	15	15	2.50 ± 0.04	N.A.	**29.2 ± 1.2**	N.A.
187,746	363	100 ± 4	0	6	69.1 ± 1.9	1	20	15	2.42 ± 0.05	35.5 ± 1.4	**28.5 ± 1.0**	1.2 ± 0.1
187,747	390	97 ± 1	0	6	74.5 ± 1.8	1	23	15	2.45 ± 0.04	31.9 ± 0.7	**30.4 ± 0.9**	1.0 ± 0.0
187,748	411	104 ± 2	1	5	81.1 ± 3.0	0	24	15	2.33 ± 0.04	35.2 ± 0.8	**34.8 ± 1.4**	1.0 ± 0.0
187,749	421	96 ± 2	0	6	75.4 ± 2.0	0	21	15	2.46 ± 0.04	33.4 ± 0.8	**30.6 ± 0.9**	1.1 ± 0.0
187,750	450	101 ± 2	1	5	78.4 ± 2.7	0	18	15	2.49 ± 0.04	34.9 ± 0.8	**31.5 ± 1.2**	1.1 ± 0.1
187,751	472	100 ± 3	0	6	85.2 ± 1.6	2	19	15	2.50 ± 0.04	34.5 ± 1.3	**34.1 ± 0.8**	1.0 ± 0.0
187,752	492	105 ± 1	0	3	84.7 ± 2.6	0	18	15	2.36 ± 0.04	37.9 ± 0.8	**35.9 ± 1.3**	1.1 ± 0.0
187,753	513	117 ± 3	0	6	87.6 ± 3.0	0	18	15	2.46 ± 0.04	37.7 ± 1.3	**35.6 ± 1.4**	1.1 ± 0.1
187,754	537	115 ± 5	0	6	84.8 ± 2.0	1	17	15	2.39 ± 0.04	37.9 ± 1.8	**35.5 ± 1.0**	1.1 ± 0.1
187,755	568	120 ± 3	1	5	97.3 ± 2.6	1	23	15	2.42 ± 0.04	42.5 ± 1.2	**40.2 ± 1.2**	1.1 ± 0.0
187,756	596	126 ± 2	0	6	92.7 ± 3.6	0	18	15	2.48 ± 0.04	40.3 ± 0.8	**37.4 ± 1.6**	1.1 ± 0.1
187,757	619	122 ± 1	0	3	100.3 ± 3.2	1	23	15	2.40 ± 0.04	43.5 ± 0.8	**41.8 ± 1.5**	1.0 ± 0.0
187,758	645	129 ± 4	0	6	96.7 ± 4.5	0	12	15	1.97 ± 0.03	54.3 ± 1.6	**49.0 ± 2.4**	1.1 ± 0.1
187,759	663	131 ± 1	0	6	103.8 ± 2.7	3	15	15	2.10 ± 0.03	52.4 ± 0.8	**49.3 ± 1.4**	1.1 ± 0.0
187,772	862	162 ± 4	0	9	113.1 ± 4.1	1	11	31	2.17 ± 0.03	57.6 ± 1.8	**52.1 ± 2.0**	1.1 ± 0.1
187,773	886	156 ± 6	0	6	100.3 ± 6.0	4	8	31	2.05 ± 0.02	52.4 ± 2.3	**48.9 ± 3.0**	1.1 ± 0.1
187,775	908	165 ± 7	0	6	93.4 ± 4.6	2	8	31	1.62 ± 0.02	64.5 ± 3.1	**57.5 ± 2.9**	1.1 ± 0.1
187,774	913	152 ± 6	0	6	90.7 ± 3.4	1	9	31	1.55 ± 0.03	60.9 ± 2.7	**58.4 ± 2.4**	1.0 ± 0.1
187,776	928	152 ± 5	0	6	113.8 ± 10.4	0	10	31	1.47 ± 0.02	63.4 ± 2.5	**77.5 ± 7.2**	0.8 ± 0.1
187,777	949	151 ± 5	0	6	103.0 ± 7.5	2	8	31	1.20 ± 0.01	70.6 ± 2.9	**85.6 ± 6.3**	0.8 ± 0.1
187,778	970	140 ± 2	2	7	90.4 ± 6.6	0	15	31	1.13 ± 0.02	67.5 ± 1.8	**79.7 ± 6.1**	0.8 ± 0.1
187,779	991	134 ± 3	0	6	71.0 ± 5.1	3	13	28	1.07 ± 0.02	66.9 ± 2.0	**66.4 ± 4.9**	1.0 ± 0.1
187,780	1048	105 ± 3	0	6	67.8 ± 4.0	1	14	28	0.78 ± 0.01	61.0 ± 2.2	**87.4 ± 5.4**	0.7 ± 0.0
187,781	1210	205 ± 10	0	6	95.7 ± 9.0	2	15	28	1.89 ± 0.03	**72.6 ± 3.7**	50.6 ± 4.8	1.4 ± 0.2
187,782	1308	217 ± 8	0	9	95.0 ± 6.7	2	14	40	1.97 ± 0.03	**82.0 ± 3.2**	48.3 ± 3.2	1.7 ± 0.1
187,783	1435	234 ± 3	0	4	153.1 ± 9.8	2	14	40	1.94 ± 0.03	**90.6 ± 1.8**	78.8 ± 5.2	1.1 ± 0.1
187,784	1553	174 ± 12	0	9	53.6 ± 4.1	2	8	40	2.01 ± 0.03	**65.5 ± 4.8**	26.7 ± 2.1	2.5 ± 0.3
187,785	1678	240 ± 11	0	6	139.2 ± 9.9	0	16	40	2.16 ± 0.03	**85.8 ± 4.1**	64.6 ± 4.7	1.3 ± 0.1
187,787	1751	211 ± 2	3	6	134.3 ± 5.5	2	14	28	1.50 ± 0.03	**98.9 ± 2.1**	89.7 ± 4.1	1.1 ± 0.1
187,788	1847	233 ± 8	1	9	155.6 ± 9.2	1	15	40	1.63 ± 0.03	**91.1 ± 3.6**	95.7 ± 5.9	1.0 ± 0.1

4.3. K-rich feldspar pIRIR ages

Typical $pIRIR_{200,290}$ dose response and stimulation (inset) curves are shown for in Fig. 4. A feldspar $pIRIR_{200,290}$ dose recovery test was carried out by adding a dose of 420 Gy on top of the natural dose for a set of 6 aliquots of sample 187,743. After subtracting the natural dose (~70 Gy) the measured to given dose ratio is 1.01 ± 0.04 (n = 6) suggesting that our chosen SAR protocol works satisfactorily. The K-rich feldspar D_e estimates ($pIRIR_{200,290}$, no residual subtraction, arithmetic averages following Guérin et al., 2017) obtained using our selected protocol are

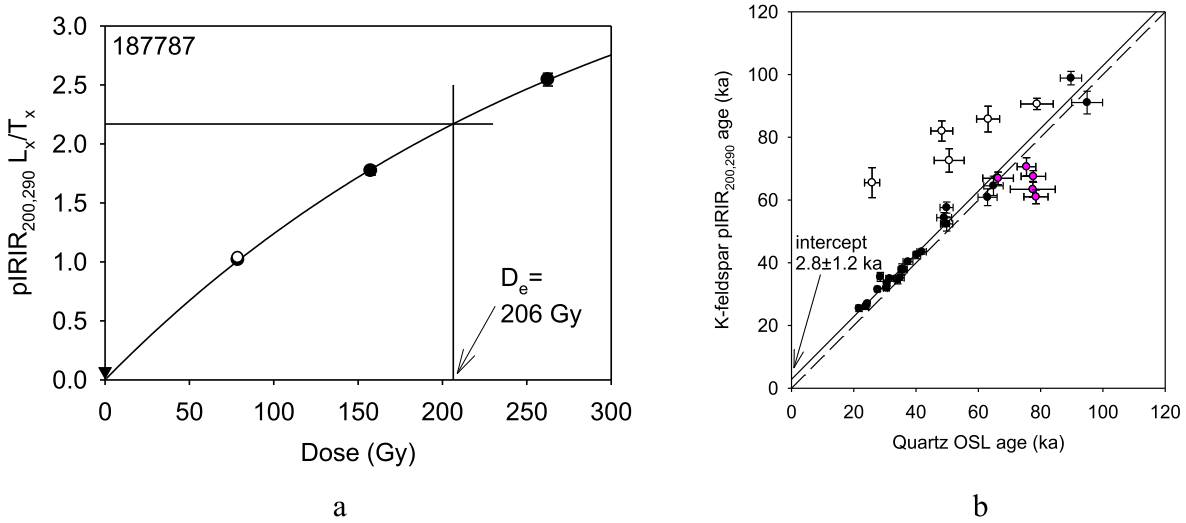

Fig. 4. (a) Typical K-feldspar grains $pIRIR_{200,290}$ dose response curve (recycled point: open circle, zero dose point: triangle) showing that even natural signals of oldest samples lie well below saturation level of the dose response curve. (b) Comparison of K-feldspar $pIRIR_{200,290}$ and quartz OSL. Both lines have unit slope, the dashed line passes through the origin, and the solid line is a fit through the data (filled circles, see text), giving an intercept of 2.8 ± 1.2 ka. Open circles are samples from the clay-rich layers (187781–85) and magenta circles are samples with quartz dose rates <1.50 Gy ka^{-1} (samples 187,776–80).

summarised in Table 1, together with the standard deviations on the means (standard errors) and the number of aliquots used to calculate the mean. The IQR criterion was used to reject outliers.

It is well-known that the $pIRIR_{290}$ signal contains a very hard-to-bleach residual component, even in loess (e.g. Buylaert et al., 2012). Here we estimate this component by comparing the feldspar $pIRIR_{200,290}$ ages with quartz OSL ages for samples that were not collected in clayey sediment (all filled symbols in Fig. 4b) or have a quartz dose rate <1.50 Gy ka^{-1} (187,741 to −74 and −87, −88; magenta symbols in Fig. 4b. The reasons for this are discussed in section 4.4 Age-depth modelling). The intercept is 2.8 ± 1.2 ka and multiplying this value by the average K-feldspar dose rate of these samples of 2.9 Gy. ka^{-1} gives a residual dose estimate of 8 ± 3 Gy. This value was subtracted from all K-feldspar D_e values before age calculation (see Table 1) and use in age-depth modelling (next section).

4.4. Age-depth modelling

It can be a seen from Fig. 4b that even though there is generally good agreement between feldspar pIRIR ages and quartz OSL ages some samples do not follow this pattern. Samples 187,781 to −85 from the clayey sediment between 1210 and 1678 cm depth have $pIRIR_{200,290}$ ages that are significantly older than the quartz ages. It can also be seen that the quartz OSL ages over this interval are very scattered and are generally too young compared to the quartz OSL ages of the samples above. We attribute this to a micro-dosimetric beta dose rate problem. The clays contained fine, presumably low-dose rate sand layers and lenses (few mm to cm thick) and these were preferentially targeted to ensure sufficient sand for measurement. But the dose rate was measured on bulk samples, which must have included some significant admixture of clay. This bulk analysis will have given the correct gamma dose rate component but the external beta dose rate component is very likely to have been overestimated and hence the quartz OSL age underestimated. The effect is much less pronounced for the $pIRIR_{200,290}$ ages over this interval, because of the dilution of this overestimation by the internal K dose rate. Therefore, for samples below 1200 cm only the feldspar ages are used for age-depth modelling (this includes the bottom two oldest samples, for which quartz and feldspar are in good agreement; Fig. 4b).

It is interesting to note that a few quartz OSL ages are older than the corresponding $pIRIR_{200,290}$ ages (magenta symbols in Fig. 4b). All these samples, despite being collected in loess, have low dose rates ranging from 0.78 ± 0.01 to 1.47 ± 0.02 Gy ka^{-1}. A similar observation has been reported by Sainz de Murieta et al. (2021) but this discrepancy is currently not well-understood. Higher fading rates for these individual samples cannot be ruled out, but we consider this very unlikely, since Költringer et al. (2022) argue for a common source for all lower Volga basin sediments. Rather, we presume this phenomenon is most likely related to inaccuracy in the measurement of the internal component of feldspar dose using IRSL signals (Buylaert et al., 2018). For all samples above 1200 cm depth the quartz OSL ages are used for age-depth modelling since the quartz OSL D_e values are well within the reliable dose range (i.e., <120 Gy) and there is no uncertainty related to the subtraction of a hard to bleach residual dose.

Age-depth modelling was carried out on a total of 35 luminescence ages measured in this paper using the R package Bacon (Blaauw and Christen, 2011). The model was run using default or suggested settings (acc.mean = 50) and the depth scale was divided into sections of equal thickness of 40 cm (thick = 40). The model was run to produce ages at 10 cm resolution. The uncertainties on the age input data only contained a random component. The Bayesian age model is shown with 1 sigma uncertainty (green uncertainty envelope) in Fig. 2, together with the interpolated model ages (with total uncertainties) at the formation boundaries.

5. Discussion

Our quartz and feldspar measurement protocols have both been shown to perform well in laboratory tests. There is a small offset in the younger feldspar ages compared to quartz, which can be explained by a difficult-to-bleach residual dose of 8 ± 3 Gy, and this was subtracted from all feldspar doses before age calculation. Two groups of ages were set aside: feldspar ages calculated using low external dose rates (<1.5 Gy/ka), and quartz ages derived from sand lenses within clay rich units – we think beta dose rates to the latter are overestimated because of fine-grain contamination of the dosimetry samples. Although we have no confident explanation for the underestimation of the feldspar group of ages, we presume it is associated with inaccurate estimation of the dose component derived from internal ^{4} K in feldspar grains (Buylaert et al., 2018). As a result, in our Bayesian modelling we have used quartz ages from the top 12 m of the section, and feldspar ages below this.

For the sake of completeness, we also present the luminescence ages from Chocolate Clays facies published previously in Kurbanov et al. (2021) after correction for improved beta source dose rate calibration (Autzen et al., submitted) (Fig. 2).

Aeolian sediments (loess and loess-like) form the middle part of Raygorod section. Költringer et al. (2021, 2022) argue that the source for loess sedimentation in this region is Volga River alluvium. The Volga River drains the central East European Plain, which is covered with middle and late Quaternary moraines sourced from Scandinavia and the Ural Mountains (Morton et al., 2003; Makshaev and Svitoch 2016; Tudryn et al., 2016). Thus, most of the material in these fine grained deposits has been transported a considerable distance, and must have been reworked many times by water and air before final sedimentation. It would appear highly likely then that these sediments were all bleached and reset before entering the Caspian Sea, rather than within the water body itself. But in any case, the completeness of bleaching of these deposits is demonstrated by the good agreement between the younger quartz OSL ages and the $pIRIR_{200,290}$ ages (e.g., Murray et al., 2012). Thus, with the exceptions noted above, we consider our individual luminescence ages reliable, and so have confidence in the resulting Bayesian chronological model.

Five stages of geomorphological development of Lower Volga valley can be identified in Raygorod section:

Stage 1 (units 21–19) is associated with an estuarine regime in the Volga valley and finishes around 90 ka (end MIS 5c). It results from a high sea level in the Caspian (the Hyrcanian transgression - Yanina et al., 2018; Kurbanov et al., 2018).

Stage 2 (units 18–14) found at the end of MIS 5 (90–76 ka) is recorded as a transition to an alluvial regime in the valley. These units were deposited in predominantly floodplain environments with periods of its stabilization and the formation of soil horizons.

Stage 3 (unit 13) is closely related to Stage 2, and resulted in sandy sediments deposited between 76 and 69 ka. This MIS 4 stage led to the formation of periglacial alluvium ("Akhtuba sands") and is coeval with the development of the Early Valdai glaciation on the East European Plain, and the Atelian regression of the Caspian Sea. The elevation of the palaeochannel of the Volga at 0–3 masl is explained by a brief increase in sea level in the Caspian, backing up the valley. This reconstruction needs further testing; because the Atelian regression is usually associated with this period (Krijgsman et al., 2019), and so channels of the Volga River should have been deeply incised in to the Northern Caspian Lowland at this time.

Stage 4 (units 12–5) is a subaerial stage with high-speed accumulation of loess during MIS 4 to MIS 2 (69–22 ka). Around 60 ka the loess accumulation rate decreases, only to increase again in the second half of MIS 3 (~41 ka). According to Költringer et al. (2020) this loess accumulation is characterized by stable cool, dry conditions. The period from 30 to 24 ka records formation of pedocomplexes at the beginning of MIS 2, and appears as three combined palaeosols. These formed under the influence of more humid conditions in the Lower Volga valley resulting

from river channel migration at altitudes 8–12 msl. When palaeosol formation stopped, there was a brief period of loess deposition after 24 ka. The record of this period is incomplete (terminates at an erosional boundary) and deposition may have continued until ~18 ka (see Stage 5).

Stage 5 (units 4–2) is clearly identified with the Khvalynian transgression (Kurbanov et al., 2021); this moved rapidly upstream and reached Raygorod at ~18 ka (Kurbanov et al., 2021). Marine erosion of the underlying loess cover was probably limited and probably affected the top 40–60 cm (extrapolated using underlying sedimentation rates); because of the very flat topography of the Northern Caspian Lowland even a modest increase in sea level results in a rapid movement of the coastline.

6. Conclusion

The luminescence characteristics of quartz OSL and post-IR IRSL signals from lower Volga sediments are satisfactory and these signals were sufficiently well reset at the time of deposition to allow accurate dating. Despite some difficulties associated with low external dose rates and clay contamination of sandy dosimetry samples compromising a few feldspar and quartz results, we are confident of our resulting chronological model for the Raygorod reference site. This detailed luminescence chronology allows us, for the first time, to reconstruct the evolution of the Lower Volga valley and identify the complex history of the Volga River channel over the last 100 ka.

From our Bayesian age-depth model we reconstruct the following phases of the Lower Volga River evolution and sedimentation history: (1) the Hyrcanian transgression of the Caspian, terminating at ~90 ka, (2) the Atelian regression, leading to alluvial sedimentation beginning ~90 ka, and level stabilization and widespread development of floodplain landscapes continuing until ~70 ka. (3) Around ~70 ka, the development of the palaeochannel intensified, and this apparently reflects a rise in sea level leading to the deposition of the Akhtuba sands. (4) From ~70 ka the Lower Volga region passed into a subaerial phase of development with the active deposition/formation of a loess-soil series terminating sometime between 22 ka and 18 ka. Soil formation was active during MIS 3c and at the beginning of MIS 2 (30–24 ka). The initial stage of soil formation is taken to reflect an increase in local moisture due to the influence of the Volga River in a brief period of a warmer climate. The second stage during MIS 2 presumably results from a similar increase in humidity, but this time from the development of a network of palaeochannels caused by a rise in the Caspian Sea level (beginning of Early Khvalynian transgression). (5) After ~18 ka, the Khvalynian transgression deposited the Chocolate clays.

Such a detailed description of the evolution of this major European river, and the links to regional, continental and global climate, is only possible because of the high spatial sampling density of our luminescence ages. This allowed the reliable identification of outliers, and the construction of a precise chronological model. In our opinion such data density is highly desirable in all similar chronological reconstructions.

Declaration of competing interest

The authors declare that they have no known competing financial interests or personal relationships that could have appeared to influence the work reported in this paper.

Acknowledgments

Taratunina, Kurbanov, Yanina, Makeev, Lebedeva and Utkina have removed their academic affiliation because sanctions following the Ukraine-Russian conflict prevent Danish researchers (Buylaert, Murray) publishing with Russian state institutions. We express our gratitude to Kristina Thomsen, Thomas Stevens and Chiara Költringer for productive discussion of the luminescence dating results, to Vicky Hansen and Warren Thompson for their enormous help in the laboratory, to Vladimir Belyaev, Alexey Rusakov and Tatiana Romanis for their help during the fieldwork and Andrei Panin and Ekaterina Badyukova for discussion of the Volga and Caspian Sea evolution. RNK was supported by grant 19-77-10077 "Chronology of the paleogeographic events of the south of the East European Plain in the Pleistocene and Holocene: new approaches and methods" (field work and geological studies), NAT was supported by grant 21-18-00552 "The earliest history of the Caspian region: chronology and development of archaeological, cultures in a changing natural environment", AOU was supported by program № AAAA-A19-119021990091-4 and TAY was supported by program № 121051100135–0.

Appendix A. Supplementary data

Supplementary data to this article can be found online at https://doi.org/10.1016/j.quageo.2022.101369.

References

Aitken, M.J., 1985. Thermoluminescence Dating. Academic Press, London.
Arslanov, K.A., Lokshin, N.V., Mamedov, A.V., 1988. On the age of Khazarian, Khvalynian and new Caspian deposits of the Caspian Sea. Bullet. Kom. Izucheniyu Chetvertichnogo Perioda 57, 28–38 (in Russian).
Arslanov, K.A., Yanina, T.A., Chepalyga, A.L., Svitoch, A.A., Makshaev, R.R., Maksimov, F.E., Chernov, S.B., Tertychniy, N.I., Starikova, A.A., 2016. On the age of the Khvalynian deposits of the Caspian Sea coast according to ^{14}C and $^{230}Th/^{234}U$ methods. Quat. Int. 409, 81–87. Part A.
Badyukova, E.N., 2021. Caspian Sea level fluctuations in the Neopleistocene (was there an Atelian regression?). Oceanology 61 (No. 2), 283–291.
Bolikhovskaya, N.S., Yanina, T.A., Sorokin, V.M., 2017. Natural environment of the Atelian epoch (according to the palynological analysis). Vestn. Mosk. Univ. Ser. 5 (No. 6), 96–101 (in Russian).
Blaauw, M., Christen, J.A., 2011. Flexible paleoclimate age-depth models using an autoregressive gamma process. Bayesian Analysis 6, 457–474.
Buylaert, J.-P., Jain, M., Murray, A.S., Thomsen, K.J., Thiel, C., Sohbati, R., 2012. A robust feldspar luminescence dating method for Middle and Late Pleistocene sediments. Boreas 41, 435–451.
Buylaert, J.-P., Yeo, E.Y., Thiel, C., Yi, S., Stevens, T., Thompson, W., Frechen, M., Murray, A.S., Lu, H., 2015. A detailed post-IR IRSL chronology for the last interglacial soil at the Jingbian site (northern China). Quat. Geochronol. 30, 194–199.
Buylaert, J.-P., Újvári, G., Murray, A.S., Smedley, R.K., Kook, M., 2018. On the relationship between K concentration, grain size and dose in feldspar. Radiat. Meas. 120, 181–187. https://doi.org/10.1016/j.radmeas.2018.06.003.
Duller, G.A.T., 2003. Distinguishing quartz and feldspar in single grain luminescence measurements. Radiat. Meas. 37, 161–165.
Fedorov, P.V., 1957. Stratigraphy of quaternary sediments and the history of the development of the Caspian Sea. Moscow. In: Trudy Geol. Inst. 10. Izd. Akad. Nauk SSSR (in Russian).
Goretskiy, G.I., 1958. On the periglacial formation. Bulletin of the commission for the study of the Quaternary period, 22. AN USSR, Moscow, pp. 4–23 (in Russian).
Goretskiy, G.I., 1966. The Development of the Volga Valley during Early and Middle Anthropogene. Nauka Press, Moscow (in Russian).
Grichuk, V.P., 1954. Materials for the paleobotanical characterization of the Quaternary and Pliocene deposits of the northwestern part of the Caspian Lowland. Mater. Po geomorfol. Paleogeograf. SSSR 11, 5–79.
Guérin, G., Mercier, N., Nathan, R., Adamiec, G., Lefrais, Y., 2012. On the use of the infinite matrix assumption and associated concepts: a critical review. Radiat. Meas. 47, 778–785.
Guérin, G., Jain, M., Thomsen, K.J., Murray, A.S., Mercier, N., 2015. Modelling dose rate to single grains of quartz in well-sorted sand samples: the dispersion arising from the presence of potassium feldspars and implications for single grain OSL dating. Quat. Geochronol. 27, 52–65.
Guérin, G., Christophe, C., Philippe, A., Murray, A.S., Thomsen, K.J., Tribolo, C., Urbanova, P., Jain, M., Guibert, P., Mercier, N., Kreutzer, S., Lahaye, C., 2017. Absorbed dose, equivalent dose, measured dose rates, and implications for OSL age estimates: introducing the Average Dose Model. Quat. Geochronol. 41, 163–173.
Hansen, V., Murray, A., Thomsen, K., Jain, M., Autzen, M., Buylaert, J.-P., 2018. Towards the origins of overdispersion in beta source calibration. Radiat. Meas. 120, 157–162.
Højsager, P., 2019. High-resolution Optically Stimulated Luminescence Dating at the Type Section Srednyaya Akhtuba, Russia. Aarhus University, Denmark. Unpublished Master Thesis.
Költringer, C., Stevens, T., Bradák, B., Almqvist, B., Kurbanov, R., Snowball, I., Yarovaya, S., 2020. Environmagnetic study of Late Quaternary environmental evolution in Lower Volga loess sequences, Russia. Quat. Res. 1–25. https://doi.org/10.1017/qua.2020.73.
Költringer, C., Bradák, B., Stevens, T., Almqvist, B., Banak, A., Linder, M., Kurbanov, R., Snowball, I., et al., 2021. Palaeoenvironmental implications from Lower Volga loess -

joint magnetic fabric and multi-proxy analyses. Quat. Sci. Rev. 267, 107057 https://doi.org/10.1016/j.quascirev.2021.107057.

Költringer, C., Stevens, T., Lindner, M., Baykal, Yu, Ghafarpour, A., Khormali, F., Taratunina, N., Kurbanov, R., 2022. Quaternary sediment sources and loess transport pathways in the Black Sea - Caspian Sea region identified by detrital zircon U-Pb geochronology. Global Planet. Change 209, 103736. https://doi.org/10.1016/j.gloplacha.2022.103736.

Krijgsman, W., Tesakov, A., Yanina, T., Lazarev, S., Danukalova, G., Van Baak, C.G.C., Agustí, J., Alçiçek, M.C., Aliyeva, E., Bista, D., Bruch, A., Büyükmeriç, Y., Bukhsianidze, M., Flecker, R., Frolov, P., Hoyle, T.M., Jorissen, E.L., Kirscher, U., Koriche, S.A., Kroonenberg, S.B., Lordkipanidze, D., Oms, O., Rausch, L., Singarayer, J., Stoica, M., van de Velde, S., Titov, V.V., Wesselingh, F.P., 2019. Quaternary time scales for the Pontocaspian domain: interbasinal connectivity and faunal evolution. Earth Sci. Rev. 188, 1–40.

Kurbanov, R.N., Svitoch, A.A., Yanina, T.A., 2014. New data on marine Pleistocene stratigraphy of the Western Cheleken peninsula. Dokl. Earth Sci. 459, 1623–1626.

Kurbanov, R.N., Yanina, T.A., Murray, A.S., Borisova, O.K., 2018. Hyrcanian epoch in the late Pleistocene history of the Manych depression. Vestnik Moskovskogo Universiteta, Seriya Geografiya 5 (3), 77–88 (in Russian).

Kurbanov, R., Murray, A., Thompson, W., Svistunov, M., Taratunina, N., Yanina, T., 2021. First reliable chronology for the early Khvalynian Caspian Sea transgression in the lower Volga River valley. Boreas 50 (No. 1), 134–146.

Lahijani, H., Tavakoli, V., Hosseindoost, M., 2007. History of Caspian environmental changes by molluscan stable isotope records. J. Coast. Res. SPEC 50, 438–442.

Lavrushin, YuA., Spiridonova, E.A., Tudryn, A., Chalié, F., Antipov, M.P., Kuralenko, N. P., Kurina, E.E., Tucholka, P., 2014. The Caspian Sea: hydrological events of the late quaternary. Bullet. Kom. Izucheniyu Chetvertichnogo Perioda 73, 19–51 (in Russian).

Lebedeva, M., Makeev, A., Rusakov, A., Romanis, T., Yanina, T., Kurbanov, R., Kust, P., Varlamov, E., 2018. Landscape dynamics in the Caspian lowlands since the last deglaciation reconstructed from the pedosedimentary sequence of Srednaya Akhtuba, southern Russia. Geosciences 8, 1–21. https://doi.org/10.3390/geosciences8120492.

Leroy, S.A.G., Lahijani, H.A.K., Djamali, M., Naqinezhad, A., Moghadam, M.V., Arpe, K., Shah-Hosseini, M., Hosseindoust, M., Miller, ChS., Tavakoli, V., Habibi, P., Naderi, M., 2011. Late little ice age palaeoenvironmental records from the Anzali and Amirkola lagoons (south Caspian Sea): vegetation and Sea level changes. Palaeogeogr. Palaeoclimatol. Palaeoecol. 302 (3–4), 415–434.

Li, B., Li, S.-H., 2012. A reply to the comments by Thomsen et al. on "Luminescence dating of K-feldspar from sediments: a protocol without anomalous fading correction". Quat. Geochronol. 8, 49–51.

Lower Volga, 2002. Geomorphology, Paleogeography and Channel Morphodynamics. GEOS, Moscow, p. 240 (in Russian).

Makeev, A., Lebedeva, M., Kaganova, A., Rusakov, A., Kust, P., Romanis, T., Yanina, T., Kurbanov, R., 2021. Pedosedimentary environments in the Caspian lowland during MIS 5 (Srednaya Akhtuba reference section, Russia). Quat. Int. 590, 164–180.

Makshaev, R.R., 2019. Paleogeography of the Middle and Lower Volga Region in during the Caspian Early Khvalyn Transgression. PhD Thesis. Lomonosov Moscow State University, Russia (in Russian).

Makshaev, R.R., Svitoch, A.A., 2016. Chocolate clays of the northern Caspian Sea region: distribution, structure, and origin. Quat. Int. 409, 44–49. Part A.

Medialdea, A., Thomsen, K.J., Murray, A.S., Benito, G., 2014. Reliability of equivalent-dose determination and age-models in the OSL dating of historical and modern palaeoflood sediments. Quat. Geochronol. 22, 11–24.

Milanovskiy, YeV., 1932. Geological Guide along the Volga: from Stalingrad to Saratov. Guided Tours of the 2nd Quaternary Geological Conference, Moscow-Leningrad (in Russian).

Milanovskiy, YeV., 1940. Essay on the Geology of the Middle and Lower Volga Region. Gostoptekhizdat, Moscow (in Russian).

Morton, A., Allen, M., Simmons, M., Spathopoulos, F., Still, J., Hinds, D., Ismail-Zadehz, A., Kroonenberg, S., 2003. Provenance patterns in a neotectonic basin: pliocene and Quaternary sediment supply to the South Caspian. Basin Res. 15, 321–337.

Moskvitin, A.I., 1962. Pleistocene of the Lower Volga Region. Trudy Geol. Inst. 64. Izd. Akad. Nauk SSSR, Moscow (in Russian).

Murray, A.S., Marten, R., Johnston, A., Martin, P., 1987. Analysis for naturally occurring radionuclides at environmental concentrations by gamma spectrometry. J. Radioanal. Nucl. Chem. 115, 263–288.

Murray, A.S., Wintle, A.G., 2000. Luminescence dating of quartz using an improved single-aliquot regenerative-dose protocol. Radiat. Meas. 32 (1), 57–73.

Murray, A.S., Wintle, A.G., 2003. The single aliquot regenerative dose protocol: potential for improvements in reliability. Radiat. Meas. 37, 377–381.

Murray, A.S., Thomsen, K.J., Masuda, N., Buylaert, J.-P., Jain, M., 2012. Identifying well-bleached quartz using the different bleaching rates of quartz and feldspar luminescence signals. Radiat. Meas. 47 (No. 9), 688–695. https://doi.org/10.1016/j.radmeas.2012.05.006.

Murray, A.S., Helsted, L.M., Autzen, M., Jain, M., Buylaert, J.-P., 2018. Measurement of natural radioactivity: calibration and performance of a high-resolution gamma spectrometry facility. Radiat. Meas. 120, 215–220.

Nikolayev, V.A., 1956. Lower Volga in Khazar time. Vestn. Mosk. Univ. Seria Biol., Soil., Geol., Geogr. 1 (in Russian).

Nikolayev, V.A., 1957. Lower Volga in Khvalynian time. Byull. MOIP 32 (4) (in Russian).

Prescott, J.R., Hutton, J.T., 1994. Cosmic ray contributions to dose rates for luminescence and ESR dating: large depths and long-term time variations. Radiat. Meas. 23, 497–500.

Rogov, V.V., Streletskaya, I.D., Taratunina, N.A., Kurchatova, A.N., Kurbanov, R.N., Yanina, T.A., 2020. Late Pleistocene cryogenesis in the lower Volga region. Vestn. Mosk. Univ. Ser. 5 (No. 6), 73–85 (In Russian).

Sainz de Murieta, E., Cunha, P.P., Cearreta, A., Murray, A.S., Buylaert, J.-P., 2021. The Oyambre coastal terrace: a detailed sedimentary record of the Last Interglacial Stage in northern Iberia (Cantabrian coast, Spain). J. Quat. Sci. 36 (No. 4), 570–585.

Shkatova, V.K., 2010. Paleogeography of the late Pleistocene Caspian basins: geochronometry, paleomagnetism, paleotemperature, paleosalinity and oxygen isotopes. Quat. Int. 225, 221–229.

Stevens, T., Buylaert, J.-P., Thiel, C., Újvári, G., Yi, S., Murray, A.S., Frechen, M., Lu, H., 2018. Ice-volume-forced erosion of the Chinese Loess Plateau global Quaternary stratotype site. Nat. Commun. 9 (983).

Svitoch, A.A., 2014. The Big Caspian: Structure and History of Development. Izd. Moskovskogo Universiteta, Moscow (in Russian).

Svitoch, A.A., Makshaev, R.R., 2015. "Chocolate" clays of the Northern Caspian: distribution, occurrence, and structure. Geomorpfologiya 4, 101–112 (in Russian).

Svitoch, A.A., Yanina, T.A., 1997. Quaternary Deposits of the Caspian Sea Coasts. RASKhN Press, Moscow (in Russian).

Taratunina, N., Rogov, V., Streletskaya, I., Thompson, W., Kurchatova, A., Yanina, T., Kurbanov, R., 2021. Late Pleistocene cryogenesis features of a loess-paleosol sequence in the Srednyaya Akhtuba reference section, Lower Volga River valley, Russia. Quat. Int. 590, 56–72.

Thomsen, K.J., Murray, A.S., Jai, M., Bøtter-Jensen, L., 2008. Laboratory fading rates of various luminescence signals from feldspar-rich sediment extracts. Radiat. Meas. 43, 1474–1486.

Tudryn, A., Chalie, F., Lavrushin, Yu A., Antipov, M.P., Spiridonova, E.A., Lavrushin, V. Yu, Tucholka, P., Leroy, S.A.G., 2013. Late quaternary Caspian Sea environment: late Khazarian and early Khvalynian transgressions from the lower reaches of the Volga River. Quat. Int. 292, 193–204.

Tudryn, A., Leroy, S.A.G., Toucanne, S., Gibert-Brunet, E., Tucholka, P., Lavrushin, YuA., Dufaure, O., Miska, S., Bayon, G., 2016. The Ponto-Caspian basin as a final trap for southeastern Scandinavian Ice-Sheet meltwater. Quat. Sci. Rev. 148, 29–43.

Vandenberghe, D., De Corte, F., Buylaert, J.-P., Kučera, J., Van den haute, P., 2008. On the internal radioactivity in quartz. Radiat. Meas. 43, 771–775.

Vasiliev, Yu.M., 1961. Antropogene of the Southern Volga Region. Academy of Science of the USSR, Moscow (in Russian).

Yanina, T.A., 2012. Correlation of the late Pleistocene paleogeographical events of the Caspian Sea and Russian plain. Quat. Int. 271, 120–129.

Yanina, T.A., Svitoch, A.A., Kurbanov, R.N., Murray, A.S., Tkach, N.T., Sychev, N.V., 2017. Experience of dating of Pleistocene deposits of the Lower Volga area by method of optically stimulated luminescence. Vestn. Mosk. Univ. Ser. 5 (No. 2), 21–29 (in Russian).

Yanina, T., Bolikhovskaya, N., Sorokin, V., Romanyuk, B., Berdnikova, A., Tkach, N., 2021. Paleogeography of the Atelian regression in the Caspian Sea (based on drilling data). Quat. Int. 590, 73–84.

Yanina, T., Sorokin, V., Bezrodnykh, Yu, Romanyuk, B., 2018. Late Pleistocene climatic events reflected in the Caspian Sea geological history (based on drilling data). Quat. Int. 465, 130–141.

Yanina, T., 2020. Environmental variability of the ponto-Caspian and Mediterranean basins during the last climatic macrocycle. Geogr. Environ. Sustain. 3 (4), 6–23.

Yi, S., Buylaert, J.-P., Murray, A.S., Thiel, C., Zeng, L., Lu, H., 2015. High resolution OSL and post-IR IRSL dating of the last interglacial-glacial cycle at the Sanbahuo loess site (northeastern China). Quat. Geochronol. 30, 200–206.

Zhao, H., Li, S.-H., 2005. Internal dose rate to K-feldspar grains from radioactive elements other than potassium. Radiat. Meas. 40, 84–93.